Journal of Hydrology 537 (2016) 419–430

Contents lists available at ScienceDirect

Journal of Hydrology

journal homepage: www.elsevier.com/locate/jhydrol

Intercomparison of selected fixed-area areal reduction factor methods

Sandra Pavlovic [a,b,*], Sanja Perica [a], Michael St Laurent [a,b], Alfonso Mejía [c]

[a] National Water Center, NWS, NOAA, Silver Spring, MD, USA
[b] University Corporation for Atmospheric Research, Boulder, CO, USA
[c] Department of Civil and Environmental Engineering, The Pennsylvania State University, University Park, PA, USA

ARTICLE INFO

Article history:
Received 21 March 2015
Received in revised form 1 March 2016
Accepted 14 March 2016
Available online 22 March 2016
This manuscript was handled by Andras Bardossy, Editor-in-Chief, with the assistance of Uwe Haberlandt, Associate Editor

Keywords:
Areal Reduction Factors
Point-to-area precipitation conversion
Areal rainfall frequency estimates
Areal precipitation frequency estimates

SUMMARY

The areal reduction factor (*ARF*) is a concept used in many hydrologic designs to transform a point precipitation frequency estimate of a given duration and frequency to a corresponding areal estimate. Various methods have been proposed in the literature to calculate *ARF*s. Proposed *ARF*s could vary significantly, and it is unclear if discrepancies are primarily due to differences in methodologies, the dissimilar datasets used to calculate *ARF*s, or if they originate from regional uniqueness.

Our goal in this study is to analyze differences among *ARF*s derived from different types of fixed-area *ARF* methods, which are suitable for use with precipitation frequency estimates. For this intercomparison, all the *ARF*s were computed using the same, high-quality rainfall-radar merged dataset for a common geographic region. The selected *ARF*s methods represent four commonly used approaches: empirical methods, methods that are based on the spatial correlation structure of rainfall, methods that rely on the scaling properties of rainfall in space and time, and methods that utilize extreme value theory. The state of Oklahoma was selected as the study area, as it has a good quality radar data and a dense network of rain gauges. Results indicate significant uncertainties in the *ARF* estimates, regardless of the method used. Even when calculated from the same dataset and for the same geographic area, the *ARF* estimates from the selected methods differ. The differences are more pronounced for the shorter durations and larger areas. Results also indicate some *ARF* dependence on the average recurrence intervals.

1. Introduction

Point precipitation frequency estimates, such as those from NOAA Atlas 14 (e.g., Perica et al., 2013), are used in many infrastructure designs in the United States (US). These estimates are representative only for a limited area around the point and as such cannot be used in many applications that require areal precipitation frequency estimates. Approximating the areal estimates by averaging corresponding point precipitation frequency estimates will result in overestimation of areal estimates, particularly for larger areas.

The areal reduction factor (*ARF*) is a concept that has been widely used in engineering design to convert point precipitation for a specified duration D [T] and frequency into areal precipitation over an area A [L^2] for the same duration and frequency. Frequency can be represented by the average recurrence interval *ARI* (also known as return period) or the annual exceedance probability *AEP* (for more information on the definition and difference between the *ARI* and *AEP*, see Perica et al., 2013). Typically, *ARF*s are presented as a set of curves showing the variation of *ARF* with A, D, and *ARI*.

*ARF*s that concur with precipitation frequency estimates are normally developed using the so-called "fixed-area" (or "geographically-fixed-area") methods. They are distinct from "storm-centered" areal reduction ratios developed based on the analysis of individual storms, which are used to convert point estimates of probable maximum precipitation to areal estimates. In this study, the focus is on fixed-area methods.

Many fixed-area methods have been proposed to date for point-to-area rainfall conversion. A comprehensive list of both fixed-area and storm-centered methods can be found in Olivera et al. (2008) and Svensson and Jones (2010). Svensson and Jones (2010) classify *ARF* methods into four main categories: (i) empirical methods (Bell, 1976; Natural Environmental Research Council, 1975; U.S. Weather Bureau, 1958), (ii) methods that are based on the spatial correlation structure of rainfall (Asquith and Famiglietti, 2000; Roche, 1966; Sivapalan and Blöschl, 1998; Srikanthan, 1995), (iii) methods that take advantage of the scaling properties of rainfall

* Corresponding author at: National Water Center, NOAA's National Weather Service, 1325 East-West Highway, SSMC Building 2, Silver Spring, MD 20910, USA.
E-mail address: sandra.pavlovic@noaa.gov (S. Pavlovic).

http://dx.doi.org/10.1016/j.jhydrol.2016.03.027
0022-1694/

in space and time (De Michele et al., 2001, 2011; Veneziano and Langousis, 2005), and (iv) methods that utilize extreme value theory (Durrans et al., 2002; Allen and DeGaetano, 2005; Lombardo et al., 2006; Olivera et al., 2008; Overeem et al., 2010).

Proposed *ARF*s could vary significantly, but since their quantitative intercomparison is lacking, it is unclear if differences are primarily due to differences in methodologies and/or the dissimilar datasets used to derive them, or if they point out to distinctive regional characteristics in the *ARF*s. The aim of this study is to analyze differences among *ARF*s from various fixed-area methods. For this comparison, one representative method from each of the four main categories listed above was selected. The selected methods were used to calculate *ARF*s for a common geographic area and using an identical dataset. More details on the study area and the dataset used are given in Section 2. Section 3 provides a review of the four selected *ARF* methods. In Section 4, we provide details on the methods' parameterization and present the *ARF*s. In Section 5, we discuss differences among the different *ARF* curves. Lastly, Section 6 summarizes the main findings and makes recommendations for future work.

2. Study area and dataset

The state of Oklahoma, with an area of 181,035 km^2, was selected as the study area, primarily due to its dense network of rain gauges and the availability of high-quality radar data (Gourley et al., 2011; Koren et al., 2004; Seo, 1998; Smith et al., 2004). Oklahoma is located in the central US between the Great Plains and the Ozark Plateau. The terrain mostly contains a gradual rise in elevation from east to west (plains), although mountain ranges such as the Ouachita Mountains and the Ozark Mountains are located in the eastern part of the state. Annual precipitation increases from west to east, from approximately 400–1650 mm. The highest annual precipitation is located in the east near the windward sides of the Ouachita and Ozark Mountain ranges. More information about the selected region is available elsewhere (Gourley et al., 2011; Seo et al., 2004; Smith et al., 2004).

To determine the *ARF*s, we used precipitation data from the National Center for Environmental Prediction's (NCEP's) Next-Generation Radar (NEXRAD) Stage IV gridded precipitation dataset (NCEP, 2014). NEXRAD is a network of 178 Doppler weather radars (WSR-88D) across the US, operated by the National Weather Service (NWS). This data are available at ~4 km resolution and at a 1-h time step.

The predominant source of uncertainty in raw radar precipitation estimates is the assumed relationship between the reflectivity and precipitation amount ('*Z*–*R* relationship'), which varies by precipitation type (e.g., Rinehart, 2004). Because precipitation is sensed well above the ground surface, precipitation detected by the radar may move large distances downwind or evaporate before reaching the ground. Further uncertainty arises from the radar technology itself, such as beam blockage and bright band errors (Rinehart, 2004). Nevertheless, weather radar data for our selected region has better than average accuracy, due to the relatively simple topography and no significant effects from snow or reservoirs (Koren et al., 2004; Seo, 1998).

Rain gauges are generally considered to provide the most accurate precipitation information at a given location, but still have limitations. These limitations include instrumental errors (Rinehart, 2004; Sieck et al., 2007) and undercatch due to wind and erratic behavior of the mechanical aspects of the gauge during intense rainfall (Lanza and Stagi, 2009; Molini et al., 2005). Also, the interpolation of point precipitation to areal precipitation is sensitive to the interpolation technique employed due to the high spatial variability of precipitation, even in areas with dense networks (Starks and Moriasi, 2009; Strangeways, 2007; Tobin and Bennett, 2009). This presents a significant challenge for *ARF* calculations, particularly at sub-daily durations.

The Stage IV precipitation data is a merge of radar and rain gauge data, meaning that the raw radar estimates have been adjusted on the basis of rain gauge data (gauge-conditioned). Such adjusted data have been shown to be consistently superior to the raw radar data (Yilmaz et al., 2005; Young et al., 2000). Although available since the 1990s, gauge-conditioned radar data are considered accurate only from 2002, when the multisensor precipitation estimation algorithm was implemented on the radar data, with rain gauge values taken from weather stations within the NWS Hydrometeorological Automated Data System network (Westcott et al., 2008). Gauge-conditioned radar data have improved over time but they are still affected by uncertainties that are both systematic and random in nature (Eldardiry et al., 2015; Villarini et al., 2014). It is, however, recognized in radar hydrology that radar data can be useful for calculating the statistics of extreme events and that spatial pooling can often be employed to compensate for having short radar records (Berne and Krajewski, 2013).

Since the statistical methods used in the calculation of precipitation frequency estimates, such as those published in the NOAA Atlas 14 Volumes (Perica et al., 2013), are typically based on the analysis of annual maximum series (AMS) data, the *ARF* methods selected for this study also make use of the AMS data. We extracted AMS for selected locations, durations and area sizes from gridded hourly Stage IV precipitation data (hereafter referred to as radar data) between 2002 and 2013. Locations at which we extracted AMS data match the locations of the 386 rain stations in Oklahoma, whose data were used in the NOAA Atlas 14 Volume 8 precipitation frequency analysis (Perica et al., 2013). The area in Oklahoma outlined in Fig. 1 was selected for this study. This area was selected by taking into consideration the climatology of heavy precipitation and precipitation mechanisms within the larger Midwestern climate region of the US. This was done as part of the development of the NOAA Atlas 14 Volume 8. Based on that analysis, the eastern Oklahoma rugged terrain areas were excluded from the climate region of the rest of the state of Oklahoma because heavy rain events in this area follow different precipitation mechanisms due to orographic effects. Additionally, the western panhandle of Oklahoma has been excluded from this analysis to keep a relatively simple regional structure.

To extract the AMS we followed an approach similar to the one used by Overeem et al. (2010). For each selected location, we identified a corresponding grid cell in the radar dataset. Then, we calculated hourly areal average precipitation for areas of 1×1, 3×3, 5×5, 7×7, and 9×9 grid cells centered at the grid cell of interest (which correspond to areal sizes of ~16, 144, 400, 784, and 1296 km^2, respectively). We analyzed *ARF*s for durations of 1-h, 2-h, 6-h, 12-h and 24-h. For durations longer than 1-h, the precipitation at each grid point was first aggregated to the 2-h, 6-h, 12-h, and 24-h duration at every hour. The area-averaged accumulations for selected durations were then calculated for each grid cell and each hour for areas of 1×1, 3×3, 5×5, 7×7, and 9×9 grid cells. Lastly, the annual maximum value was extracted independently for each duration and area size, allowing different AMS for different area sizes and durations at the same grid point. With the assumption that the whole study area is homogeneous with respect to the characteristics of extreme precipitation, we combined the corresponding annual maxima from all locations into a single AMS with a total length of 4632 (hereafter referred to as regional AMS). This was done for each combination of area size and duration. Fig. 1 illustrates the AMS extraction process.

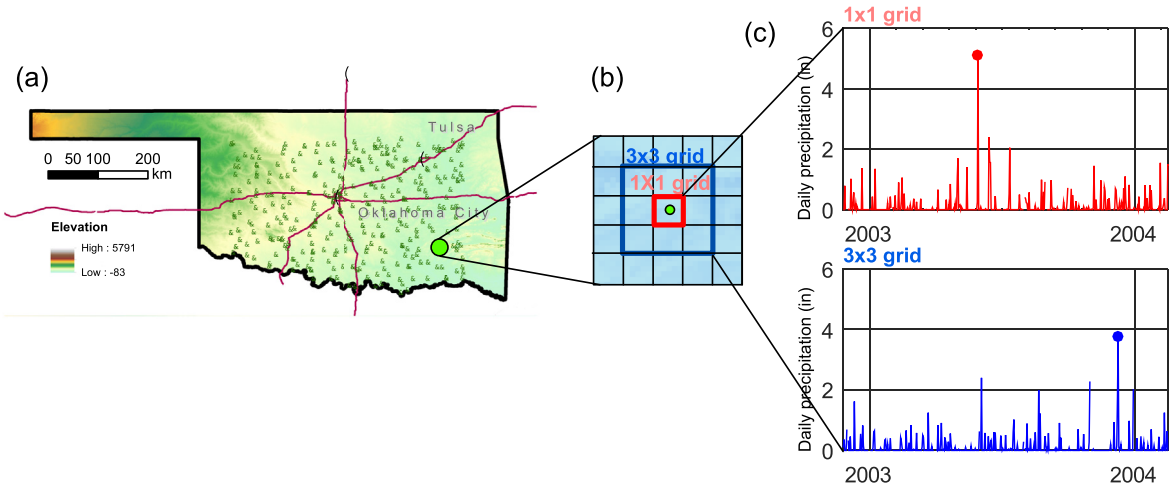

Fig. 1. (a) Selected locations in the study area for which AMS data were extracted. (b) Illustration of the approach used to extract areal average precipitation. For each selected location and for each selected duration, areal average precipitation was calculated by averaging gridded radar data for 1×1, 3×3, 5×5, 7×7 and 9×9 boxes, centered at the location. Since the native radar data is hourly, native data was aggregated to different durations prior to determining the areal average precipitation. (c) For each location, the AMS data were extracted from the areal average precipitation for different combinations of duration and area sizes.

3. Review of selected *ARF* methods

We selected the following methods to represent the 4 main types of fixed-area *ARF* methods: (i) a variation of the US Weather Bureau (1958) method for empirical methods (hereafter referred to as the M1 method), (ii) Sivapalan and Blöschl (1998) method for methods that are based on the spatial correlation structure of rainfall (M2 method), (iii) De Michele et al. (2001) method to represent methods that rely on the notion of scaling and statistical self-affinity (M3 method), and (iv) the method proposed by Overeem et al. (2010) for methods that utilize extreme value theory (M4 method).

3.1. M1 method

The M1 method is based on the original empirical *ARF* method developed by the NWS predecessor (US Weather Bureau, 1958). The Weather Bureau developed a set of curves to transform point rainfall to areal rainfall for durations between 1 and 24 h and areas up to 1000 km^2. These *ARF*s (hereafter referred to as ARF_{WB}) were assumed to be independent of the average recurrence interval. ARF_{WB} were estimated using the data from several rain gauge networks located in different geo-climatic regions and are applicable to the whole US. The number of gauges in each network varied from 5 to 13 (over areas of ~800 km^2) and their record lengths varied from 7 to 15 years. It is relevant to note that, despite the fact that many new methods have been proposed since 1958, the ARF_{WB} curves are still commonly used in engineering design in the US.

We implemented the Weather Bureau's approach for *ARF* calculation with one modification regarding the extraction of areal AMS. Areal AMS in the Weather Bureau's method were calculated as averages of corresponding AMS at gauged locations, while here we first created areal rainfall grids from the original radar grids and then used them to extract areal AMS at selected locations.

The *ARF* from method M1 (ARF_1) is computed as

$$ARF_1(D,A) = \frac{P(D,A)}{P(D,A^*)}, \tag{1}$$

where P [L] is the depth of the mean areal annual maximum precipitation for selected area A and duration D, and A^* denotes the area of a single grid cell. Similarly to the Weather Bureau's method, M1 does not account for *ARI*, and consequently, the ARF_1 curves are assumed to be applicable across all *ARI*s.

3.2. M2 method

The Sivapalan and Blöschl (1998) method (M2 method) utilizes the spatial correlation structure of rainfall for the *ARF* derivation. An assumption is made that the point parent rainfall is exponentially distributed and that the areal average parent rainfall is Gamma distributed (Sivapalan et al., 1990; Wood and Hebson, 1986; Yoo et al., 2007). The variance of the areal average rainfall is set equal to the product of the variance of the point rainfall and the variance reduction factor κ^2, which is given by (Rodriguez-Iturbe and Mejía, 1974)

$$\kappa^2 = \int_0^{R_{max}} \rho(r) f_R(r) dr, \tag{2}$$

where r [L] is the distance between any two points randomly chosen within a square area A [L^2], $\rho(r)$ is the spatial correlogram, $f_R(r)$ is the probability distribution for distance R (i.e., the random variable whose realization is r), and R_{max} is the maximum possible distance between any two points in A. A mathematical expression for $f_R(r)$ is given by Ghosh (1951). Eq. (2) has no analytical solution, thus it must be solved numerically.

Different functions can be used to model the spatial correlogram (e.g., exponential, nested double-exponential, nested exponential function) (Blöschl and Sivapalan, 1997; Bras and Rodríguez-Iturbe, 1985; Sivapalan and Blöschl, 1998; Sivapalan et al., 1990). Here we use the correlogram proposed and used with rain gauge data in central Oklahoma by Ciach and Krajewski (2006) and Mandapaka et al. (2009),

$$\rho(r) = \exp[-(r/\lambda)^c], \tag{3}$$

where λ [L] is the spatial correlation length and c is the power exponent. The selection of the spatial correlogram is further discussed in Section 4.2.

For the AMS data, the point and areal values are both assumed to follow a Gumbel distribution. First, the maximum likelihood approach is used on the "point" regional AMS data to obtain the scale α^* [L^{-1}] and location μ^* [L] parameters of the Gumbel distribution for each duration D. The "point" regional AMS data refers to the regional AMS data at the smallest spatial scale implied by the

data. For radar data, this is the area of a single grid cell, A^*. The following functions are then used to relate the distribution parameters with the duration

$$\alpha^* = a_\alpha + b_\alpha D^{c_\alpha}, \quad \text{and} \tag{4}$$

$$\mu^* = a_\mu + b_\mu D^{c_\mu}, \tag{5}$$

where a_α, b_α, c_α, a_μ, b_μ, and c_μ are fitting parameters.

The Gumbel distribution parameters for the areal AMS, α_A [L^{-1}] and μ_A [L], are defined as follows (Sivapalan and Blöschl, 1998)

$$\alpha_A = \alpha^* \kappa^{-2}[1 - 0.17\ln(\kappa^{-2})], \quad \text{and} \tag{6}$$

$$\mu_A = \mu^* \kappa^{-2}[0.39 + 0.61(\kappa^{-2})^{0.8}]. \tag{7}$$

All the parameters in Eqs. (6) and (7) were defined previously.

Lastly, using the inverse of the Gumbel cumulative distribution function, together with Eqs. (2)–(7), the *ARF* for method M2 (ARF_2) can be expressed as follows

$$ARF_2(D, A, ARI) = \frac{\alpha^*\left\{\alpha_A\mu_A - \ln\left[-\ln(1 - ARI^{-1})\right]\right\}}{\alpha_A\left\{\alpha^*\mu^* - \ln\left[-\ln(1 - ARI^{-1})\right]\right\}}, \tag{8}$$

Notice that the dependence of ARF_2 in Eq. (8) on A and D is implicit through the dependence of α_A and μ_A on A (through κ) and of α^* and μ^* on D.

3.3. M3 method

The M3 method (De Michele et al., 2001) uses the concepts of dynamic scaling and statistical self-affinity to find a general expression for the mean annual maxima P as a function of the rainfall duration D and area A. The *ARF* from method M3 (ARF_3) is computed by fitting a general expression to the ARF_1 estimates. Similar to method M1, M3 does not account for *ARI*, and therefore the ARF_3 from Eq. (14) is applicable across all *ARI*s.

In M3, an assumption is made that the rainfall field has dynamic scaling properties expressed through the following relationship

$$\frac{D_j}{D_l} = \left(\frac{A_j}{A_l}\right)^z, \tag{9}$$

where z ($z > 0$) is the dynamic scaling exponent, and the subscripts j and l represent different scales. The rainfall field $i(D,A)$ [L/T], which represents the intensity parametrized in time and space through duration D and area A, follows a condition of statistical self-affinity by combining Eq. (9) and an assumption of scale invariance in the statistical sense:

$$\{i(\zeta^a D, \zeta^b A)\} \overset{d}{=} \zeta^{-H}\{i(D, A)\}, \tag{10}$$

where $\zeta = A_j/A_i$, $a (a > 0)$ and $b = az^{-1}$ are scaling exponents, and H ($H > 0$) is a constant known as the Hölder exponent. The notation $\{.\} \overset{d}{=} \{.\}$ indicates that the two underlying probability distributions are equal (after rescaling by a factor).

Accordingly, the average rainfall intensity i [L/T] ($i = P/D$) is equal to

$$i(D, A) = D^{-v} g\left(\frac{A^a}{D^b}\right), \tag{11}$$

where $v = H/a$. Based on asymptotic and scaling arguments, $g(\cdot)$ can be represented by

$$g\left(\frac{A^a}{D^b}\right) = a_1\left[1 + \omega\left(\frac{A^z}{D}\right)^b\right]^{-v/b}, \tag{12}$$

where a_1 and v can be obtained using

$$i(D, A^*) = a_1 D^{-v} \tag{13}$$

and ω [$T^b L^{-2a}$] is a normalization constant. A^* is the smallest spatial scale implied by the data, a single radar grid cell in this case.

Combining Eqs. (11) and (12), and dividing by (13), the *ARF* from the M3 method (ARF_3) is equal to

$$ARF_3(D, A) = \left[1 + \omega\left(\frac{A^z}{D}\right)^b\right]^{-v/b}. \tag{14}$$

Eq. (14) is calibrated to the ARF_1 estimates and requires the estimation of four parameters (v, b, ω, and z).

3.4. M4 method

For the M4 method (Overeem et al., 2009, 2010), the *ARF*s are estimated from precipitation frequency estimates obtained by fitting the Generalized Extreme Value (GEV) distribution, $F(P)$, to the mean regional AMS data P for each combination of chosen duration D and area size A. The GEV is given by

$$F(P) = \begin{cases} \exp\left\{-\left[1 + \frac{k}{\alpha}(P - \mu)\right]^{-1/k}\right\} & \text{for } k \neq 0, \\ \exp\left\{-\exp\left[-\frac{(P-\mu)}{\alpha}\right]\right\} & \text{for } k = 0, \end{cases} \tag{15}$$

where μ [L], α [L] ($\alpha > 0$), and k are the location, scale, and shape parameters of the GEV distribution, respectively. We used the maximum likelihood approach, as recommended by Overeem et al. (2010), to estimate the GEV distribution parameters.

For each duration, the following empirical relationships are used to account for the dependency of the GEV distribution parameters on the area size

$$\mu_A = a_\mu A^2 + b_\mu A + c_\mu, \tag{16}$$

$$\alpha_A = a_\alpha + b_\alpha A + c_\alpha, \quad \text{and} \tag{17}$$

$$k_A = a_k \ln A + b_k, \quad \text{for } A > 0. \tag{18}$$

where a_μ, a_α, a_k, b_μ, b_α, b_k, c_μ and c_α are parameters that need to be estimated empirically from the GEV distribution parameters. Eqs. (16)–(18) used in the M4 method are different from the ones used by Overeem et al. (2010). Their equations account explicitly for the dependence of the GEV parameters on both, A and D. In this case, we found that fitting a separate set of equations to each duration results in more reliable *ARF* estimates. This is discussed further in Section 4.4.

Lastly, by inverting Eq. (15), the relationship between the precipitation magnitude and both the area and frequency, for each duration, is given by

$$P(A, ARI) = \begin{cases} \mu_A + \frac{\alpha_A\left\{\left[-\ln(1 - ARI^{-1})\right]^{-k_A} - 1\right\}}{k_A} & \text{for } k \neq 0, \\ \mu_A - \alpha_A ln[-\ln(1 - ARI^{-1})] & \text{for } k = 0, \end{cases} \tag{19}$$

and the *ARF* can be calculated as

$$ARF_4(D, A, ARI) = \frac{P(D, A, ARI)}{P(D, A^*, ARI)}, \tag{20}$$

where ARF_4 indicates the *ARF* from the M4 method.

4. Results

In this section, we present the *ARF* curves for each of the four methods evaluated in this study. We analyzed *ARF*s for the 1-h, 2-h, 6-h, 12-h and 24-h durations but, for clarity, results are shown and discussed for the 1-h and 24-h durations only. Similarly,

results for the methods M2 and M4, which account for the *ARF* dependence on the *ARI*, are shown only for the 2-yr and 100-yr *ARI*.

4.1. ARF_1 curves

Fig. 2 shows the ARF_1 curves for the 1-h and 24-h durations, with the corresponding ARF_{WB} curves. To reveal the range of variability in the ARF_1, we also show the ARF_1 curves calculated separately for each of the 386 selected locations. Since the *ARF*s in both the Weather Bureau and M1 method are assumed independent of the *ARI*, the ARF_{WB} and ARF_1 curves should be considered valid across all *ARI*s.

The ARF_1 is consistently more conservative than the ARF_{WB} and the difference between the two is more pronounced for the shorter durations (Fig. 2). For example, for $A = 500$ km^2, the difference between ARF_1 and ARF_{WB} for the 24-h duration is ~0.04 (0.96 and 0.92, respectively) while for the 1-h duration is ~0.12 (0.79 and 0.67, respectively). Although the ARF_{WB} method was applied on the point gauge data and the highest resolution for the ARF_1 method was the area of a single grid cell, we attribute the differences between the values of ARF_1 and ARF_{WB} primarily to the different datasets used to estimate these *ARF*s. The ARF_1 is based on NEXRAD Stage IV data, which is the most recent gauge-conditioned hourly radar precipitation data available at ~4 km grid resolution and captures spatial information reasonably well. While the ARF_{WB} were estimated from interpolated grids and sparse rain gauges with measurements collected before 1960s and over very few years. Additionally, in the M1 method, we used only Oklahoma data, while in the Weather Bureau's study, data comes from gauge networks from different parts of the US.

4.2. ARF_2 curves

The application of the M2 method requires the estimation of seven parameters (κ^2, a_α, b_α, c_α, a_μ, b_μ, c_μ). To estimate the value for the variance reduction factor κ^2, the correlation length λ needs to be determined first based on the AMS data at the single grid cell scale (A^*). For the data analyzed, the spatial correlogram function from Eq. (3) provided the best fit among all the different functions tested, where the c parameter was estimated to be 0.8 for the 24-h duration and 0.62 for the 1-h duration. Fig. 3(a) and (b) shows the correlograms for the 24-h and 1-h durations, respectively, together with the correlation coefficients calculated between the mean AMS data for each pair of the 386 selected locations. Although Eq. (3) provides a reasonably good fit with a coefficient of variation R^2 of 0.94 and 0.87 for the 24-h and 1-h duration, respectively, there is significant scatter around the fitted curves. The correlation lengths λ (indicated by the vertical red lines in Fig. 3) were estimated to be ~221 km for the 24-h duration and 45 km for the 1-h duration.

To estimate κ^2, we solved Eq. (2) numerically using the solution for $f_R(r)$ derived by Ghosh (1951). Table 1 summarizes the κ^2 values for selected combinations of D and A. To estimate the remaining parameters (i.e., a_α, b_α, c_α, a_μ, b_μ, c_μ), we first calculated the scale and location parameters of the Gumbel distribution, for each duration, at the single grid cell scale (α^* and μ^*). We then fitted Eqs. (4) and (5) to these data. The fitted equations are shown in Fig. 4. The R^2 values associated with Fig. 4(a) and (b) were in both cases ~0.99. The estimated values of a_α, b_α, c_α, a_μ, b_μ and c_μ were 4.0608, 42.6485, −1, 0, 0.044, and 1, respectively. Together with the κ^2 values shown in Table 1, these parameters values were used to find α_A and μ_A for selected area sizes (Eqs. (6) and (7)) and, lastly, to calculate the values of ARF_2 for *ARI*s between 2 and 100 years.

In Fig. 5, we show the ARF_2 curves for the 24-h and 1-h durations and for the 2-yr and 100-yr *ARI*s. From this figure, the ARF_2 values decrease relatively fast for areas up to ~300 km^2, after that, they continue to decrease but at a slower rate. In addition, we calculated the ARF_2 curves separately for each of the 386 selected locations and from these curves we determined error bars for one standard deviation. The error bars in Fig. 5 are relatively narrow since for this method only the point and not the areal precipitation data are used. Fig. 5 also shows that the dependence of ARF_2 on the *ARI* is relatively weak (particularly for the 24-h duration) but statistically significant when uncertainty, represented by the error bars, is considered. For example, for 24-h duration and $A = 1000$ km^2, the difference between the 2-yr and 100-yr ARF_2 is 0.02 (0.94 and 0.92 respectively). For 1-hr duration, the difference is more significant and for the same area it is about 0.06.

4.3. ARF_3 curves

The M3 method requires the estimation of four parameters (v, b, ω, and z). First, we estimated the parameter v by fitting the power law function between the single-grid cell mean regional annual

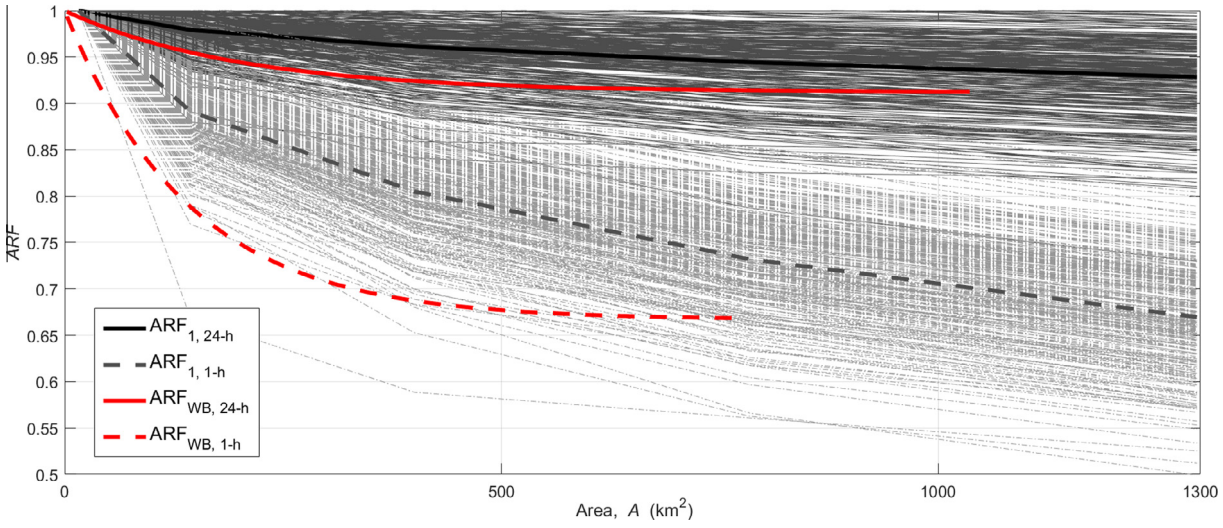

Fig. 2. ARF_1 and ARF_{WB} curves for the 1-h and 24-h durations for areas up to 1300 km^2. To illustrate the spread around the mean values, we also show the individual *ARF* curves for the M1 method for each of the selected sites. (For interpretation of the references to colour in this figure legend, the reader is referred to the web version of this article.)

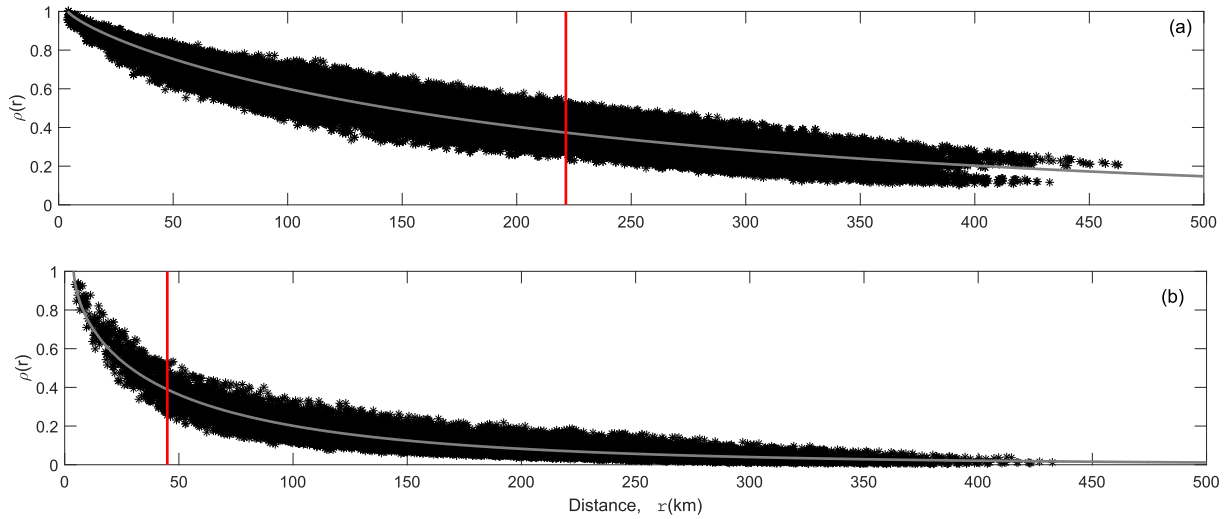

Fig. 3. Spatial correlogram $\rho(r)$ for the M2 method for the (a) 24-h and (b) 1-h duration. The red lines indicate the estimates of the spatial correlation length λ. (For interpretation of the references to colour in this figure legend, the reader is referred to the web version of this article.)

Table 1
Variance reduction factor κ^2 for the M2 method as a function of the duration D and area A.

κ^2		A (km^2)				
		16	144	400	784	1296
D (h)	24	0.9767	0.9456	0.9195	0.8963	0.8749
	12	0.9526	0.9040	0.8675	0.8370	0.8101
	6	0.9285	0.8623	0.8155	0.7777	0.7454
	2	0.8903	0.7964	0.7331	0.6837	0.6428
	1	0.8662	0.7548	0.6811	0.6244	0.5781

maxima for each of the 5 selected durations and the corresponding durations (Eq. (13)) using nonlinear regression. The fitted function, with parameter values $a_1 = 37.40$ [mm h^{-1}] and $v = 0.697$, provided a nearly perfect fit with $R^2 = 0.99$. We then estimated the remaining three parameters (b, ω, and z). For this, we fitted Eq. (14) directly to the empirical *ARF*s derived from the radar data (i.e., ARF_1). We simultaneously fitted the 5 different *ARF* curves representing each of the 5 durations considered. This fitting was done using a version of the Nelder–Mead optimization algorithm (Lagarias et al., 1998). For the objective function, we used the mean of the squared errors e^2, as follows

$$e^2 = \frac{1}{N_D}\frac{1}{N_A}\sum_{p=1}^{N_D}\sum_{j=1}^{N_A}[ARF_3(D_p, A_j) - ARF_1(D_p, A_j)]^2, \quad (21)$$

where the subscripts j and p represent different area sizes and durations, respectively. N_A and N_D are the total number of different area sizes and durations, respectively; in this case both N_A and N_D are equal to 5. Notice that in order to determine the error in Eq. (21), we needed an estimate of ARF_1 for each combination of area size and duration. A similar objective function to Eq. (21) was successfully used by Koutsoyiannis et al. (1998) for fitting Intensity–Duration–Frequency curves. The parameter values obtained for b, ω, and z were 0.5985, 0.004, and 1.0914, respectively.

Fig. 6 shows the regional ARF_3 curves from Eq. (14) for the 24-h and 1-h durations together with error bars representing one standard deviation of the site specific results. The error bars were determined using the *ARF* curves associated with each of the 386 selected locations. Since method M3 does not account for the

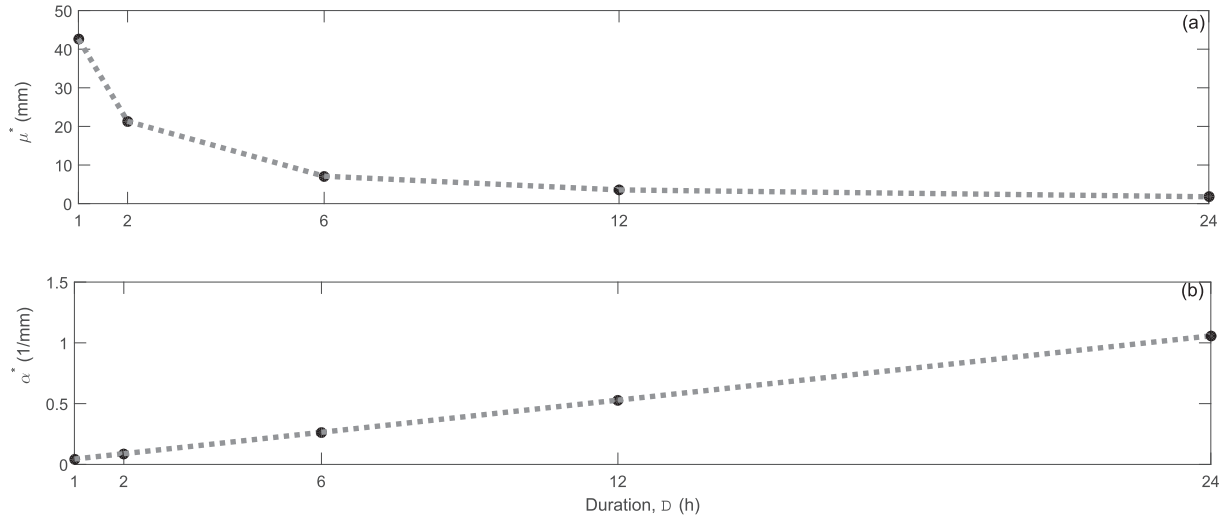

Fig. 4. Parameters for the Gumbel distribution as a function of the duration D: (a) μ^* versus D, and (b) α^* versus D. These parameters are used in the M2 method (see, e.g., Eqs. (4) and (5)).

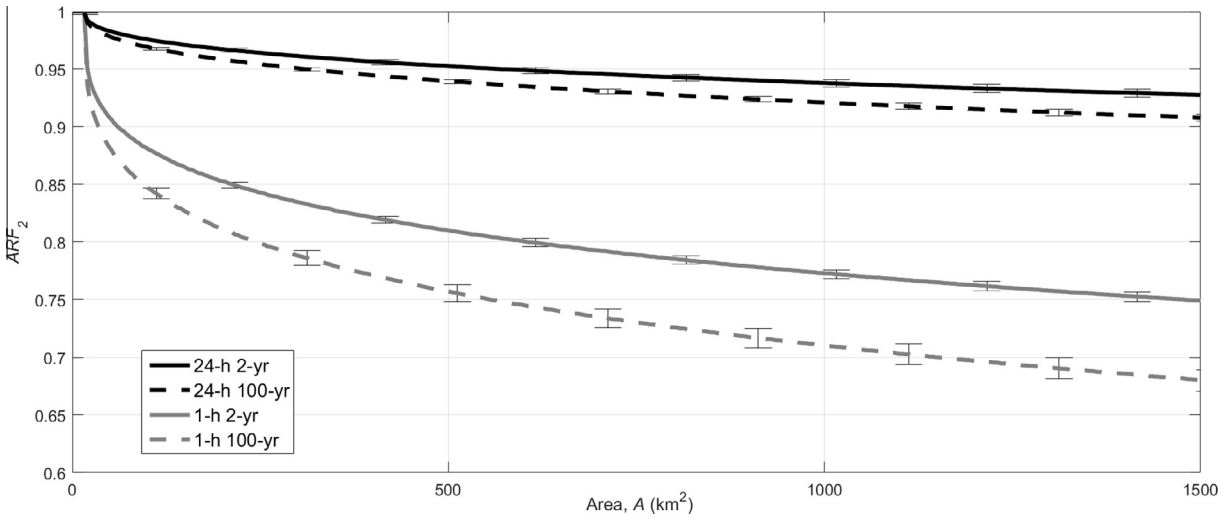

Fig. 5. ARF_2 curves for the 2-yr and 100-yr *ARI*s and 24-h and 1-h durations. The error bars indicate ±1 standard deviation computed based on the estimation of the ARF_2 at each of the selected sites.

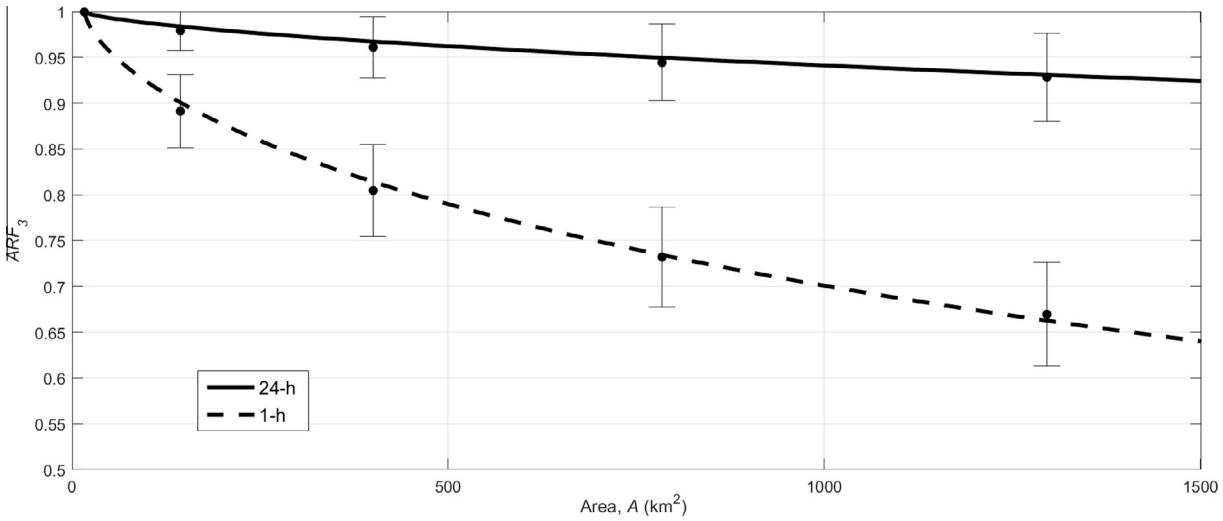

Fig. 6. ARF_3 curves for the 24-h and 1-h durations. The ARF_1 empirical estimates are also shown as dots. The M3 method does not account for the possible dependence of the *ARF* on the *ARI*. The error bars indicate ±1 standard deviation computed based on the estimation of the ARF_3 at each of the selected sites.

effects of the *ARI*s on the *ARF*s, the ARF_3 curves in Fig. 6 are considered applicable across all *ARI*s. Overall, the fits in Fig. 6 are reasonable but, as the error bars indicate, there is significant spread around the ARF_3 curves.

4.4. ARF_4 curves

To implement the M4 method, we first estimated the GEV distribution parameters μ, α and k from Eq. (15) using the maximum likelihood method, together with the areal AMS data for each combination of selected area size and duration. For each duration, we then found the parameters a_μ, a_α, a_k, b_μ, b_α, b_k, c_μ and c_α in the empirical Eqs. (16)–(18), which describe the dependency of the GEV parameters on the area size. To estimate these parameters, we again used a version of the Nelder–Mead optimization algorithm, which was used before for the M3 method, with the objective function shown in Eq. (21). This time the errors were computed as the difference between the GEV parameters obtained by the maximum likelihood approach and the corresponding parameters obtained from Eqs. (16)–(18). The fitting of Eqs. (16)–(18) is illustrated in Fig. 7(a–c) for parameters α_A, μ_A, and k_A, respectively. For all three parameters, the R^2 values for all the fitted curves are above 0.98. For the shape parameter k_A, we used a single equation to represent all the durations, as we did not find any appreciable gains in using separate equations. Additionally, we tried different equations when fitting the GEV parameters to the areas, but Eqs. (16)–(18) provided the best fits. The parameters from Eqs. (16)–(18) are summarized in Table 2.

Eq. (19) was used to determine precipitation frequency estimates for selected area sizes and *ARI*s for a given duration. These estimates were used in Eq. (20) to find the *ARF*s as a function of *A*, *D*, and *ARI*. These estimates are shown in Fig. 8 for the 2-yr and 100-yr *ARI*s. Fig. 8 reveals the ARF_4 dependence on *ARI*. The 100-yr *ARF* estimates are lower than the corresponding 2-yr estimates across all the analyzed durations and areas and the difference can be as large as 8% for the larger area sizes. Fig. 8 also shows the error bars for 1 standard deviation of the site specific curves, calculated based on the ARF_3 for each of the 386 selected locations for both the 24-h and 1-h durations and for the corresponding 2-yr and 100-yr *ARI*s. The error bars indicate that the spread around the regional estimates can be significant.

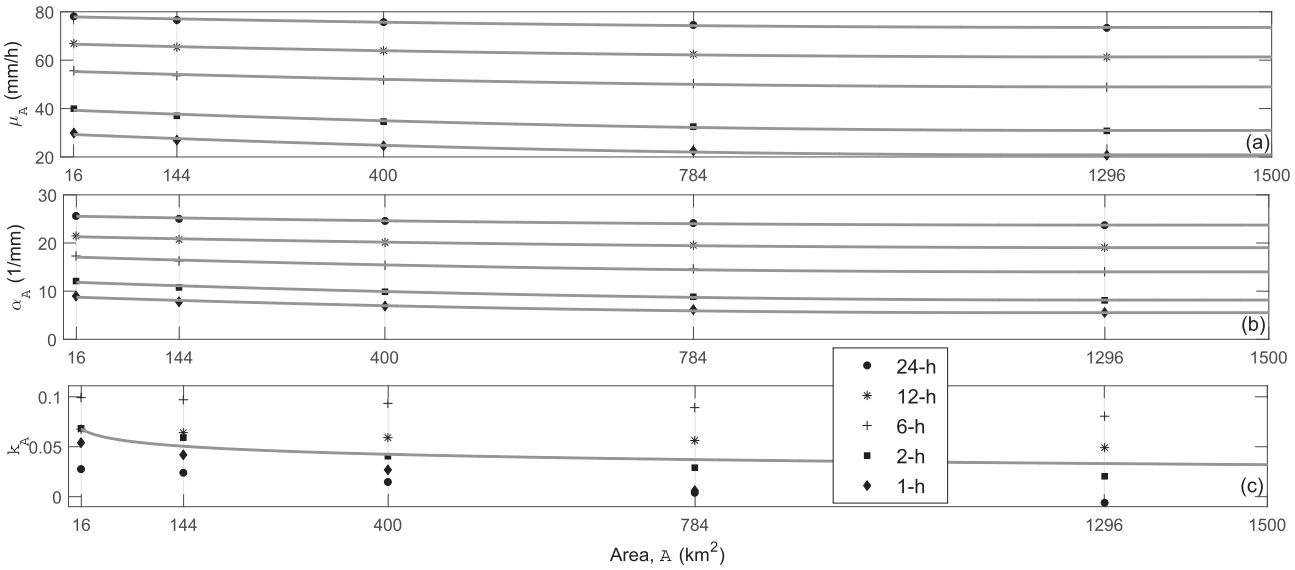

Fig. 7. Parameters for the GEV distribution as a function of the area for selected durations: (a) μ_A versus A, (b) α_A versus A, and (c) k_A versus A. For μ_A and α_A, a separate curve is fitted for each duration. For k_A, a single curve is fitted for all the durations.

Table 2
Coefficients for the empirical Eqs. (16)–(18) from the M4 method. These equations describe the dependence of the parameters from the GEV distribution (μ_A, α_A, and k_A) on the area size A.

D (h)	a_μ	b_μ	c_μ	a_α	b_α	c_α	a_k	b_k
24	2.56E−06	−0.0067	77.9733	1.13E−06	−0.0029	25.5984	−2.80E−05	0.0610
12	3.22E−06	−0.0083	66.7251	1.28E−06	−0.0034	21.3492	−2.80E−05	0.0610
6	3.81E−06	−0.0100	55.4610	2.02E−06	−0.0050	17.1404	−2.80E−05	0.0610
2	5.30E−06	−0.0135	39.4948	2.34E−06	−0.0059	11.9268	−2.80E−05	0.0610
1	5.66E−06	−0.0140	29.4940	2.35E−06	−0.0056	8.8337	−2.80E−05	0.0610

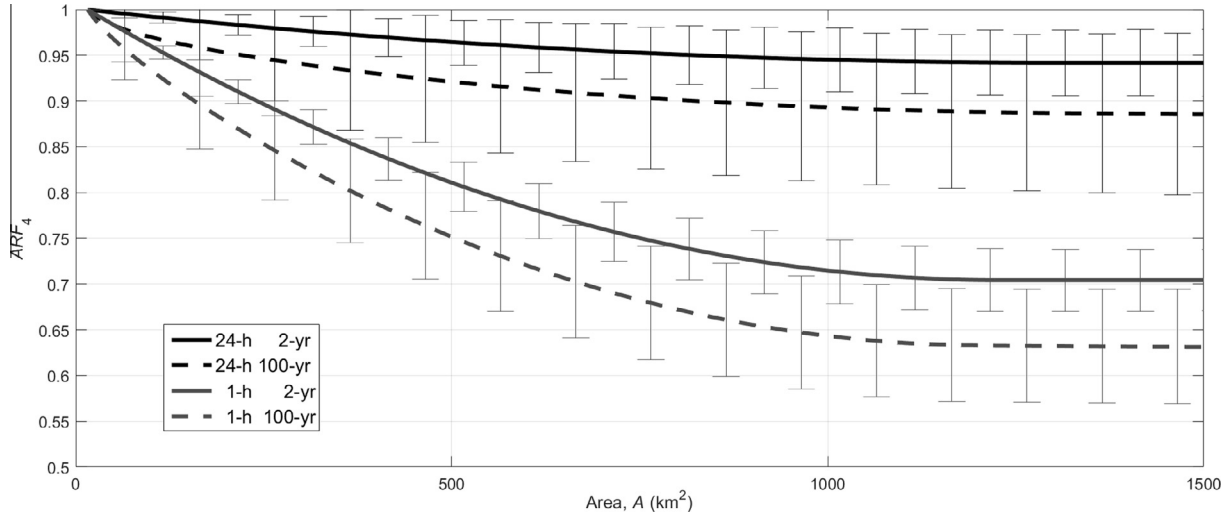

Fig. 8. ARF_4 curves for the 2-yr and 100-yr *ARI*s and the 24-h and 1-h durations. The error bars indicate ±1 standard deviation computed based on the estimation of the ARF_4 at each of the selected sites.

5. Intercomparison of *ARF*s

In this section, we compare the *ARF* estimates from the four selected methods. The comparison is done first for the *ARF*s calculated using the mean AMS and then for the *ARF*s calculated using the precipitation frequency estimates for the 2-year and 100-yr *ARI*s.

5.1. Comparison of ARFs calculated using the mean AMS

In Fig. 9(a) and (b), we show the *ARF* curves, which were derived using the 4 selected methods, for the mean annual maxima, together with the original Weather Bureau's *ARF* curves for the 24-h and 1-h durations, respectively. Fig. 9(a) shows that for the 24-h duration the *ARF* curves from all the four methods are similar. The ARF_{WB}

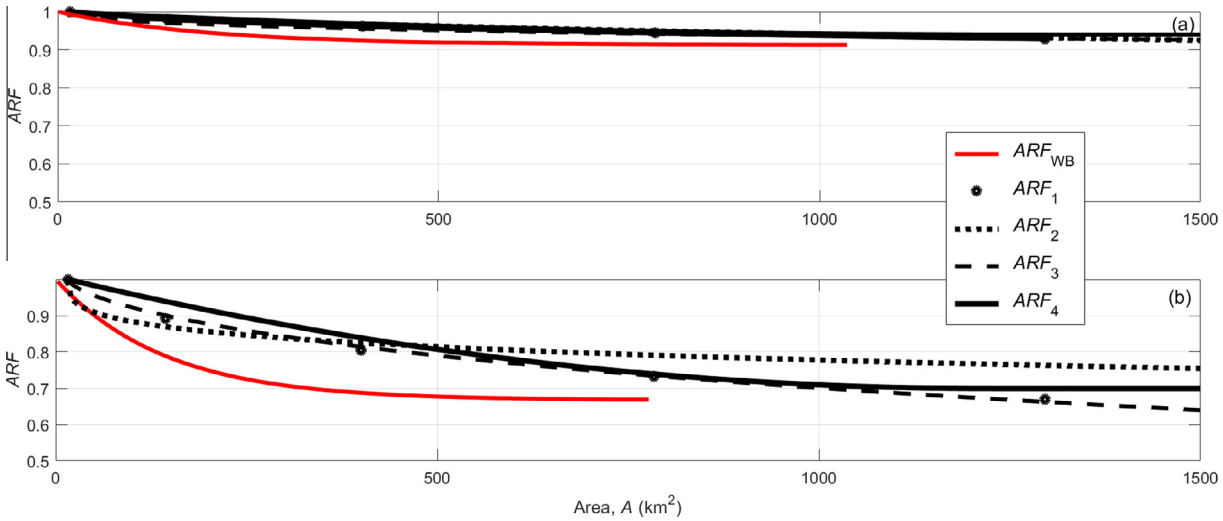

Fig. 9. *ARF* curves for the mean annual maxima and for the (a) 24-h and (b) 1-h durations. (For interpretation of the references to colour in this figure legend, the reader is referred to the web version of this article.)

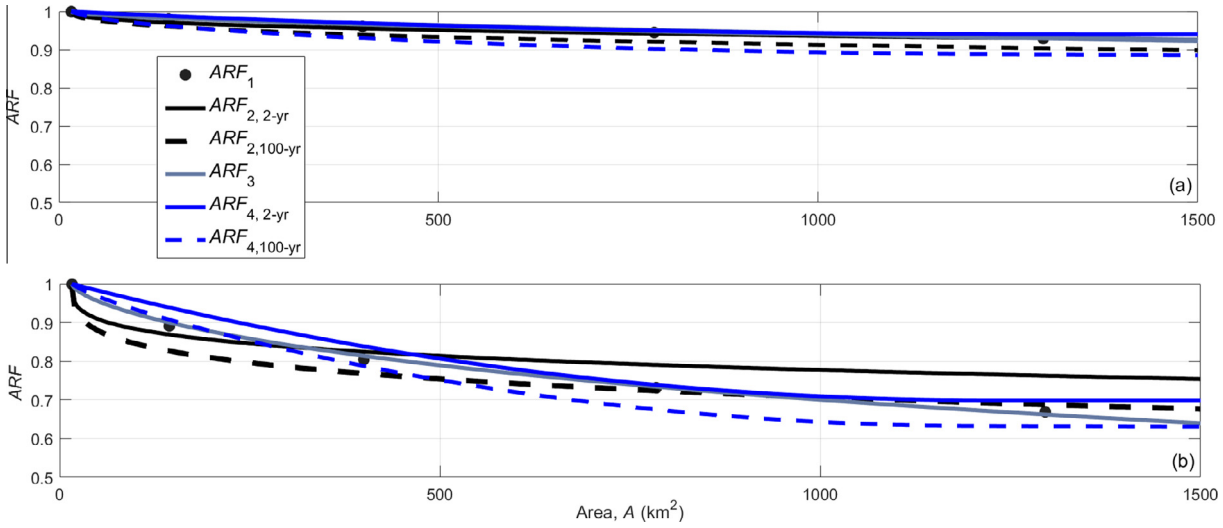

Fig. 10. *ARF* curves for the 2-yr and 100-yr *ARI*s and for the (a) 24-h and (b) 1-h durations. (For interpretation of the references to colour in this figure legend, the reader is referred to the web version of this article.)

estimates are slightly lower than the estimates from the other methods, but the differences are relatively small. For example, for $A = 500$ km^2, ARF_1, ARF_2, ARF_3 and ARF_4 are equal to 0.96, 0.95, 0.95, and 0.95, respectively, and the corresponding ARF_{WB} is 0.92.

For the 1-h duration (Fig. 9(b)), differences are more pronounced. ARF_{WB} decreases much faster than the *ARF*s from the other methods, including ARF_1, even though the Weather Bureau's and M1 methods are fundamentally the same (as discussed in Section 3.1, we attributed differences between the M1 and the Weather Bureau's method primarily to differences in the AMS data used to estimate ARF_1 versus the data used for ARF_{WB}). The ARF_1 and ARF_3 curves are relatively close to each other, which is not surprising as the ARF_1 estimates were used to calibrate the parameters of the M3 method. The ARF_2 estimates decrease faster than the *ARF*s from M1, M3, and M4 for areas up to ~300 km^2, but for larger area sizes the decline is very gradual and, for areas greater than 600 km^2, the ARF_2 estimates are larger than the estimates from any of the other methods. For $A = 750$ km^2, for example, ARF_1, ARF_2, ARF_3 and ARF_4 are equal to 0.75, 0.8, 0.75, and 0.75, respectively and the corresponding ARF_{WB} is noticeably lower at 0.69.

5.2. ARF dependence on the ARIs

Among the 4 selected methods, only two (M2 and M4) are built to account for the potential dependence of the *ARF* on *ARI*. For the other methods, we assumed that the *ARF*s calculated for the mean annual maxima apply across all *ARI*s. Due to the limited number of data years (12 years), we limited the analysis to *ARI*s to be between 2 and 100 years. In Fig. 10(a) and (b), we show the ARF_2 and ARF_4 curves for the 2-year and 100-year precipitation frequency estimates for the 24-h and 1-h durations, respectively. The *ARF* curves from the other methods are also shown for reference purposes. For the 24-h duration (Fig. 10(a)), the effect of the *ARI* is generally very small. For example, for $A = 1500$ km^2, the difference between the *ARF*s for the 2-yr and 100-yr *ARI* is about 0.03 for ARF_2 and about 0.06 for ARF_4. The *ARF*s from the other methods match closely the ARF_2 and ARF_4 curves for the 2-yr *ARI*.

For the 1-h duration (Fig. 10(b)), the influence of *ARI* on the *ARF* is more prominent. The difference between the *ARF* for the 2-yr and 100-yr *ARI* varies with the area but, generally, it is about 0.08 for both the M2 and M4 method. For the selected study area, the

ARF_1 and ARF_3 curves, which were developed based on the analysis of the mean AMS, fall within the range of the 2-yr and 100-yr ARF_2 and ARF_4 curves.

6. Summary and conclusions

The *ARF* is a concept used in many engineering designs to transform a point precipitation frequency estimate of a given duration and frequency to a corresponding areal estimate. Typically, *ARF*s are presented as a set of curves showing their variation with area, duration, and average recurrence interval (also called return period).

Many *ARF* curves have been proposed in the literature and they can vary considerably. Our goal with this study was to understand if there would still be significant discrepancies in the *ARF*s when different methods are used on the same dataset for the same geographic region. We calculated *ARF*s using four different methods that represent the most commonly used fixed-area *ARF* approaches (which are suitable for use with precipitation frequency estimates): (i) for empirical methods, we used a variation of the US Weather Bureau's (1958) method (M1 method); (ii) for methods that are based on the spatial correlogram of rainfall, we used Sivapalan and Blöschl (1998) method (M2 method); (iii) for methods that rely on the notion of scaling, we employed De Michele et al. (2001) method (M3 method); and (iv) for methods that utilize extreme value theory, we followed Overeem et al. (2010) approach (M4 method). In addition, all *ARF*s were contrasted to the original US Weather Bureau's *ARF*s, which are still commonly used in engineering applications in the US.

We selected the state of Oklahoma as the study area, primarily due to its relatively dense network of rainfall gauges and availability of high-quality radar data. Quality controlled precipitation data from 386 rain gauges was readily available to us from the NOAA Atlas 14 Volume 8 precipitation frequency project (Perica et al., 2013). We derived initial *ARF* curves from the rain gauge data only, but we observed that the spatial interpolation method had a significant influence on the *ARF*s, especially at the hourly durations. As a result, for this study, we decided to use an hourly rain, gauge-radar merged, gridded precipitation product (NCEP's Stage IV), available for the period between 2002 and 2013.

From the Stage IV data, we created areal rainfall grids and used them to extract areal AMS at 386 locations that matched the locations of the rain gauges from the NOAA Atlas 14 Volume 8. The AMS were extracted for areas between 16 km^2 (corresponding to a single grid cell area) to 1296 km^2 (9×9 grid cells) at 1-h, 2-h, 6-h, 12-h and 24-h durations. AMS were then used in the four selected methods to calculate the *ARF*s.

ARF analysis based on only 12 years of Stage IV data is likely the most significant limitation of this study. Similar to what has been done in some previous studies (e.g., Overeem et al., 2010), we sought to overcome this limitation by using a regional approach in calculating *ARF* curves. The regional approach pools data from all locations inside a delineated homogeneous region, as opposed to using data from a single site, thus creating a larger dataset and supporting the estimation of more reliable *ARF*s. One concern with this approach is the homogeneity of the selected region. To delineate our homogeneous region, we relied on previous regionalization work done as part of the development of the NOAA Atlas 14 Volume 8 products (Perica et al., 2013). However, to further demonstrate that the region selected for this study is homogeneous with respect to the *ARF*, we divided the region into four sub-regions of similar size and computed empirical *ARF* curves for each sub-region for the 1-hr and 24-h durations. The corresponding sub-regional *ARF* curves (not shown) matched each other closely and they all agreed well with the corresponding *ARF* curves derived for the whole region. Thus, we concluded that the selected region could be considered homogenous with respect to the *ARF*.

Another potential concern that can arise from using gridded precipitation products that are derived from merged radar and gauged data, such as the Stage IV data, has to do with quality of the data itself. To address this concern, we compared for our selected region the daily *ARF* curve based on the merged Stage IV data against the *ARF* curve from a gauged-derived product. For the gauged-derived product, we used the PRISM data (PRISM, 2014). From this comparison (figure not shown), we found that the daily *ARF* curves obtained using the Stage IV and PRISM data match each other closely. Thus, we deemed the use of the Stage IV data in this case reasonable. However, this may not be the case in other locations.

In this study, we first compared *ARF* curves calculated from the averages of the AMS data and contrasted them to the Weather Bureau's curves. We also looked at the range of uncertainties in the *ARF* curves. This analysis revealed several important conclusions:

- For all the methods, there is significant scatter of the individual *ARF* curves (calculated at 386 selected locations) around the corresponding regional *ARF* curves, which indicates a significant amount of uncertainty in the regional *ARF* estimates.
- For the 24-h duration, the *ARF*s from all the four methods were alike for all the area sizes analyzed. The differences became more pronounced as the duration decreased.
- For the selected study area, the *ARF* estimates from all the four methods were more conservative than the corresponding Weather Bureau's estimates across all the durations and area sizes considered. The difference is most significant at the 1-h duration where the Weather Bureau's *ARF*s are about 0.1–0.2 lower than the *ARF*s from any of the other methods considered here.
- The M1 method follows the same approach as the US Weather Bureau's method, but the *ARF*s from the two methods differ. We attributed these differences primarily to the data used to estimate the *ARF*s. However, since the Bureau's curves were calibrated on rain gauge data from across the whole US, they may also point to some regional uniqueness of the *ARF*s.
- The *ARF* estimates from the M2 method depend strongly on the spatial correlogram function and its correlation length parameter. We observed differences in these *ARF*s of 0.15 or more depending on the choice of this function. Additionally, choosing this function is complicated by the significant scatter of the correlation coefficients around the fitted curve. On the other hand, the key advantage of this method is that it does not require areal precipitation data, thus allowing the use of point precipitation data from rain gauges with long record lengths.
- The M3 method, which relies on scaling arguments, was the most straightforward to implement among the 3 theoretical *ARF* methods (M2, M3, and M4). In the M3 method, a single scaling equation, which requires the estimation of very few parameters, is needed to reproduce the *ARF*s. For the selected study area, the scaling equations were flexible enough to match the empirical *ARF*s across all the analyzed area sizes and durations. However, the generality of the M3 should be further assessed by implementing the M3 method in other regions with different climatic characteristics.
- The M4 method has a significant advantage over the other methods that, in essence, it follows the frequency analysis approach used in many precipitation frequency studies, including the NOAA Atlas 14. This could potentially facilitate the consistent and more efficient transfer of information (e.g., the GEV distribution parameters) between the point precipitation frequency and *ARF* studies. The M4 method is somewhat more

involved to implement than the other methods as it requires calibration of many empirical parameters to develop relationships between the GEV parameters and the area. However, based on this study, we do not foresee that this would be a problem in other applications as the relationships have a simple form and yielded very good fits. The main disadvantage of the M4 method is that the *ARF* accuracy depends considerably on the record length, as relatively long records are needed for reliable frequency analysis. This problem will diminish as the sample size of the radar data increases.

We also examined the *ARI*'s influence on the *ARF*. Due to the limited number of years in the data, we narrowed this analysis to *ARIs* between 2 and 100 years. Since the M1 and M3 method disregard the *ARI*'s influence on the *ARF*, for these two methods we assumed that the *ARF*s calculated using the mean annual maxima apply across all the *ARIs*. The methods M2 and M4 show that even with significant uncertainties in the estimates, the *ARI*'s influence on the *ARF* should be accounted for, as there is a clear separation of the *ARF* curves with longer *ARIs*. The dependency of the *ARI* on the *ARF* is more pronounced for the shorter durations.

In conclusion, the choice of the *ARF* method has a marked influence on the *ARF* estimates, especially for the hourly durations. The differences among the *ARF*s from the different methods are more pronounced for the larger areas and for longer *ARI*s.

We plan to duplicate this work in other regions to test the influence of geographical variations on the *ARF*s. Regions with different extreme precipitation climatology are expected to have distinct characteristics of point and areal AMS data and precipitation frequency estimates, but it still remains to be seen if that has a statistically significant influence on the *ARF*s.

Acknowledgements

We are thankful for the support and assistance provided by the Hydrometeorological Design Studies Center's team at NOAA's NWS while carrying out this research. We are thankful to the two anonymous reviewers for their constructive comments and suggestions, they helped improve the overall quality of the manuscript.

References

Allen, R.J., DeGaetano, A.T., 2005. Considerations for the use of radar-derived precipitation estimates in determining return intervals for extreme areal precipitation amounts. J. Hydrol. 315, 203–219.
Asquith, W.H., Famiglietti, J.S., 2000. Precipitation areal-reduction factor estimation using an annual-maxima centered approach. J. Hydrol. 230 (1–2), 55–69.
Bell, F.C., 1976. The Areal Reduction Factor in Rainfall Frequency Estimation, Report Number 35. Institute of Hydrology, Wallingford, UK.
Berne, A., Krajewski, W.F., 2013. Radar for hydrology: unfulfilled promise or unrecognized potential? Adv. Water Resour. 51, 357–366.
Blöschl, G., Sivapalan, M., 1997. Process controls on regional flood frequency: coefficient of variation and basin scale. Water Resour. Res. 33 (12), 2967–2980.
Bras, R.L., Rodríguez-Iturbe, I., 1985. Random Functions and Hydrology. Dover Publications, Canada.
Ciach, G.J., Krajewski, W.F., 2006. Analysis and modeling of spatial correlation structure in small-scale rainfall in Central Oklahoma. Adv. Water Resour. 29 (10), 1450–1463.
De Michele, C., Kottegoda, N.T., Rosso, R., 2001. The derivation of areal reduction factor of storm rainfall from its scaling properties. Water Resour. Res. 37 (12), 3247–3252.
De Michele, C., Zenoni, E., Pecora, S., Rosso, R., 2011. Analytical derivation of rain intensity–duration–area–frequency relationships from event maxima. J. Hydrol. 399 (3–4), 385–393.
Durrans, S., Julian, L., Yekta, M., 2002. Estimation of depth-area relationships using radar-rainfall data. J. Hydrol. Eng. 7 (5), 356–367.
Eldardiry, H., Habib, E., Zhang, Y., 2015. On the use of radar-based quantitative precipitation estimates for precipitation frequency analysis. J. Hydrol. 531 (2), 441–453.
Ghosh, B., 1951. Random distances within a rectangle and between two rectangles. Bull. Calcutta Math. Soc. 43, 17–24.
Gourley, J., Hong, Y., Flamig, Z., Wang, J., Vergara, H., Anagnostou, E., 2011. Hydrologic evaluation of rainfall estimates from radar, satellite, gauge, and combinations on Ft. Cobb Basin, Oklahoma. J. Hydrometeorol. 12 (5), 973–988.
Koren, V., Reed, S., Smith, M., Zhang, Z., Seo, D.-J., 2004. Hydrology laboratory research modeling system (HL-RMS) of the US national weather service. J. Hydrol. 291 (3–4), 297–318.
Koutsoyiannis, D., Kozonis, D., Manetas, A., 1998. A mathematical framework for studying rainfall intensity-duration-frequency relationships. J. Hydrol. 206 (1–2), 118–135.
Lagarias, J., Reeds, J., Wright, M., Wright, P., 1998. Convergence properties of the Nelder–Mead Simplex method in low dimensions. SIAM J. Optim. 9 (1), 112–147.
Lanza, L.G., Stagi, L., 2009. High resolution performance of catching type rain gauges from the laboratory phase of the WMO Field Intercomparison of Rain Intensity Gauges. Atmos. Res. 94 (4), 555–563.
Lombardo, F., Napolitano, F., Russo, F., 2006. On the use of radar reflectivity for estimation of the areal reduction factor. Nat. Hazards Earth Syst. Sci. 6, 377–386.
Mandapaka, P.V., Krajewski, W.F., Ciach, G.J., Villarini, G., Smith, J.A., 2009. Estimation of radar-rainfall error spatial correlation. Adv. Water Resour. 32 (7), 1020–1030.
Molini, A., Lanza, L.G., La Barbera, P., 2005. The impact of tipping-bucket raingauge measurement errors on design rainfall for urban-scale applications. Hydrol. Process. 19 (5), 1073–1088.
National Center for Environmental Prediction (NCEP), 2014. Next-generation radar (NEXRAD) Stage IV gridded precipitation dataset.
National Environment Research Council, 1975. Flood Studies Supplementary Report No 1: The Areal Reduction Factor In Rainfall Frequency Estimation, UK.
Olivera, F., Choi, J., Kim, D., Li, M., 2008. Estimation of average rainfall areal reduction factors in Texas using NEXRAD data. J. Hydrol. Eng. 13 (6), 438–448.
Overeem, A., Buishand, T.A., Holleman, I., 2009. Extreme rainfall analysis and estimation of depth-duration-frequency curves using weather radar. Water Resour. Res. 45 (10) W10424.
Overeem, A., Buishand, T.A., Holleman, I., Uijlenhoet, R., 2010. Extreme value modeling of areal rainfall from weather radar. Water Resour. Res. 46 (9) W09514.
Perica, S., Martin, D., Pavlovic, S., Roy, I., St Laurent, M., Trypaluk, C., Unruh, D., Yekta, M., Bonnin, G., 2013. NOAA Atlas 14 Volume 8, Precipitation-frequency Atlas of the United States, Midwestern States. NOAA, National Weather Service, Silver Spring, MD.
PRISM Climate Group, 2014. <http://www.prism.oregonstate.edu/recent/> (accessed on July 5, 2014).
Rinehart, R.E., 2004. Radar for Meteorologists. Rinehart Publications.
Roche, M., 1966. Hydrologie de Surface. Gauthier-Villars, Paris.
Rodriguez-Iturbe, I., Mejía, J.M., 1974. On the transformation of point rainfall to areal rainfall. Water Resour. Res. 10 (4), 729–735.
Seo, D.J., 1998. Real-time estimation of rainfall fields using radar rainfall and rain gage data. J. Hydrol. 208 (1–2), 37–52.
Seo, D.J., Koren, V., Reed, S.M., Zhang, Z., Duan, Q., Moreda, F., Cong, S., 2004. The distributed model intercomparison project (DMIP): motivation and experiment design. J. Hydrol. 298 (1–4), 4–26.
Sieck, L.C., Burges, S.J., Steiner, M., 2007. Challenges in obtaining reliable measurements of point rainfall. Water Resour. Res. 43 (1) W01420.
Sivapalan, M., Blöschl, G., 1998. Transformation of point rainfall to areal rainfall: intensity-duration-frequency curves. J. Hydrol. 204 (1–4), 150–167.
Sivapalan, M., Wood, E.F., Beven, K.J., 1990. On hydrologic similarity: 3. A dimensionless flood frequency model using a generalized geomorphologic unit hydrograph and partial area runoff generation. Water Resour. Res. 26 (1), 43–58.
Smith, M.B., Sea, D.J., Koren, V., Reed, S.M., Zhang, Z., Dian, Q., Moredo, F., Cong, S., 2004. The distributed model intercomparison project (DMIP): motivation and experiment design. J. Hydrol. 298 (1–4), 4–26.
Srikanthan, R., 1995. A Review of the Methods for Estimating areal Reduction Factors for Design Rainfalls. Cooperative Research Centre for Catchment Hydrology.
Starks, P.J., Moriasi, D.N., 2009. Spatial resolution effect of precipitation data on SWAT calibration and performance: implications for CEAP. Trans. ASAE (Am. Soc. Agric. Eng.) 52 (4).
Strangeways, I., 2007. Precipitation: Theory, Measurement and Distribution. Cambridge University Press, New York, NY.
Svensson, C., Jones, D.A., 2010. Review of methods for deriving areal reduction factors. J. Flood Risk Manage. 3 (3), 232–245.
Tobin, K.J., Bennett, M.E., 2009. Using SWAT to model streamflow in two river basins with ground and satellite precipitation data1. J. Am. Water Resour. Assoc. 45 (1), 253–271.
U.S. Weather Bureau, 1958. Rainfall intensity-frequency regime – Part 2. In: Commerce, U.D.O. (Ed.), Technical Paper No. 29, Washington, DC.
Veneziano, D., Langousis, A., 2005. The areal reduction factor: a multifractal analysis. Water Resour. Res. 41 (7) W07008.
Westcott, N.E., Knapp, H.V., Hilberg, S.D., 2008. Comparison of gage and multi-sensor precipitation estimates over a range of spatial and temporal scales in the Midwestern United States. J. Hydrol. 351 (1–2), 1–12.
Villarini, B., Seo, B.-C., Serinaldi, F., Krajewski, W.F., 2014. Spatial and temporal modeling of radar rainfall uncertainties. Atmos. Res. 135–136, 91–101.

Wood, E.F., Hebson, C.S., 1986. On hydrologic similarity: 1. Derivation of the dimensionless flood frequency curve. Water Resour. Res. 22 (11), 1549–1554.
Yoo, C., Kim, K., Kim, H.S., Park, M.J., 2007. Estimation of areal reduction factors using a mixed Gamma distribution. J. Hydrol. 335 (3–4), 271–284.
Yilmaz, K.K., Hogue, T.S., Hsu, K., Sorooshian, S., Gupta, H.V., Wagener, T., 2005. Intercomparison of rain gauge, radar, and satellite-based precipitation estimates with emphasis on hydrologic forecasting. J. Hydrometeorol. 6 (4), 497–517.
Young, C.B., Bradley, A.A., Krajewski, W.F., Kruger, A., Morrissey, M.L., 2000. Evaluating NEXRAD multisensor precipitation estimates for operational hydrologic forecasting. J. Hydrometeorol. 1 (3), 241–254.